Investigating the Interoperability of Unsymmetrical Charging Coils for Unmanned Aerial Vehicles

Sushan PRADHAN, Avishek MUNSI, and Kunwar ADITYA

***Abstract*—This paper investigates the interoperability of unsymmetrical transmitter (Tx) and receiver (Rx) coil geometries for wireless charging of unmanned aerial vehicles (UAVs). It evaluates the coupling performance of circular, double-D (DD), and bipolar (BP) coil structures under various excitation modes to identify configurations that minimize sensitivity to misalignment. The study analyses BP coils under both 0° and 180° excitation modes and DD coils in a conventional configuration. Finite element analysis (FEA) using Ansys Maxwell and experimental validation through hardware implementation were conducted to examine magnetic coupling across air gaps (10 to 100 mm) and lateral misalignments (±250 mm). The interoperability assessment identified the circular Tx-Rx coil pair as the most robust solution, achieving a nominal coupling coefficient ($k \approx 0.2$) at a 50 mm air gap with misalignment tolerance of ±50 mm in both x and y directions. BP (0°) excitation mode demonstrated improved misalignment tolerance but required a reduced air gap for optimal coupling, while DD configurations showed stronger coupling along specific misalignment axes but were more sensitive to positional deviations. The findings emphasize the importance of coil geometry and excitation mode in enhancing UAV wireless charging performance. This research provides comprehensive guidelines for optimizing Tx-Rx coil interoperability, with the circular coil pair emerging as the most effective design for stable and efficient power transfer under real-world misalignment conditions.**

***Index Terms*—Bipolar pad, charging coil, interoperability, misalignment tolerance, resonant inductive power transfer (RIPT), unmanned aerial vehicle (UAV), wireless power transfer (WPT).**

I. Introduction

UNMANNED aerial vehicle (UAV), commonly referred to as drones, have limited flight range of 20 to 30 min. Wireless power transfer (WPT) presents a promising solution for extending its flight time through autonomous, opportunistic, and drone to drone charging features [1]–[5]. As shown in Fig. 1, a typical wireless charging system consists of a transmitter (Tx) at the charging base station and a receiver (Rx) mounted on the UAV, with power transfer facilitated via resonant inductive coupling. The system comprises multiple components, including power converters, a charge controller, a battery management system (BMS), a communication interface, foreign object detection (FOD), and a resonant inductive link. The resonant inductive link consists of compensation capacitors and a loosely coupled Tx-Rx coil pair. These loosely coupled coils are the key components that distinguish a wireless charger from a conventional plug-in charger. Their design and optimization are crucial for achieving efficiency comparable to traditional wired charging. Additionally, it is this loose coupling that enables the advantage of cordless charging, eliminating the need for user intervention and allowing fully autonomous operation. However, designing these coils presents challenges due to the non-linear behavior of magnetic materials, complex geometries, and stringent design constraints.

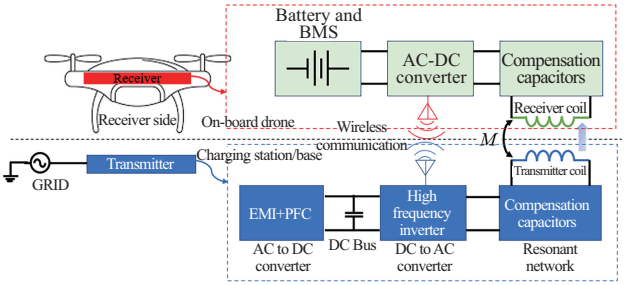

Fig. 1. Illustration of a WPT system for UAV charging applications.

Recent research in WPT has increasingly emphasized the importance of coil interoperability, where diverse coil types, sizes, and compensation methods must reliably work together under practical constraints. Zhang et al. proposed an asymmetrical quadrupolar coil interoperable with four conventional coil types, boosting interoperability for efficient WPT across misaligned and diverse geometries [6]. [7] investigated coil designs and misalignment tolerance, revealing robust strategies for maintaining performance across varied operational scenarios, particularly for electric vehicle (EV) charging. Other studies provide experimental insight into interoperable unipolar Tx coils, identifying critical features for reliable operation across multiple misaligned Tx arrangements [8]. Rahman et al. and Yoon et al. summarized advances in multifunctional and mixed-coil platforms, highlighting trends toward practical interoperability in multi-device charging systems [9], [10]. Additionally, studies in [11] and [12] reported on bidirectional WPT interoperability, emphasizing the role of mutual coupling and coil topology in

Manuscript received June 2, 2025; revised October 31, 2025 and December 26, 2025; accepted March 3, 2026. Date of publication June 30, 2026; date of current version April 27, 2026. No funding was received to assist with the preparation of this manuscript. (*Corresponding author: Kunwar Aditya.*)

All authors are with the Transportation Electrification Lab (T.E.L), Electrical Engineering Department, Indian Institute of Technology, Rajasthan 342037, India (e-mail: pradhan.5@iitj.ac.in; p22ee004@iitj.ac.in; kunwar.aditya@iitj.ac.in).

Digital Object Identifier 10.24295/CPSSTPEA.2026.00009

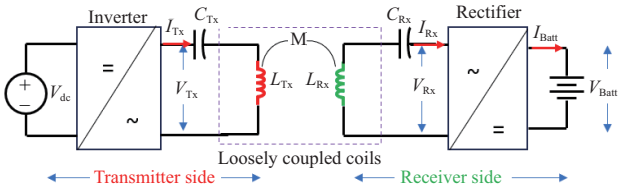

Fig. 2. Equivalent circuit of the charger.

achieving high-efficiency charging.

Despite these advances, most existing studies on coil interoperability have been centered on EVs, where weight and space constraints are less critical. These works often employ hybrid or multi-geometry symmetrical coil combinations to improve interoperability, increasing system complexity and cost. This study focuses on a simplified two coil topology one Tx and one Rx specifically designed for UAV wireless charging, where Rx weight and geometry are tightly constrained due to available space, load capacity and shape of drone. While several UAV studies have adopted solenoid coils mounted on the landing gear, this work employs planar coils owing to their lightweight structure, ease of integration, and low manufacturing cost. This study presents the experimental investigation and validation of unsymmetrical Tx-Rx coil pairs, quantifying interoperability, efficiency, and misalignment tolerance under realistic conditions. The findings offer practical design guidelines for scalable, lightweight, and low-cost UAV charging infrastructure.

Thus, this paper focuses on the coil design aspect of the wireless charger, with the primary objective of identifying Tx-Rx coil pairs that are less sensitive to coupling variations, specifically for UAV charging applications. To evaluate interoperability, parameters of wireless charger were calculated for a 5200mAh 5S 25C/50C (18.5V) lithium polymer battery pack, a commonly used power source in UAVs. System parameters were calculated based on a series-series (SS) resonant inductive link fed by a voltage source inverter, as illustrated in Fig. 2. The key parameters of the charger are summarized in Table I. The detailed design steps for calculating these parameters have been previously published in [13] and will not be repeated here.

It should be noted that for resonant inductive links, various compensation topologies can be used, including multiresonant topologies such as LCC, LCL, and CLC, as well as two-element resonant topologies like SS, series-parallel (SP), parallel-series (PS), and parallel-parallel (PP) [14]–[17]. Multiresonant topologies require additional components, making them unsuitable for UAV applications due to limited onboard space and the need to keep the Rx as lightweight as possible. Among the two-element resonant topologies, SS topology achieves the highest peak efficiency while also being the only topology unaffected by load and coupling variations [18]–[20]. This makes it particularly suitable for wireless charging applications where misalignment is common. Furthermore, when supplied with a fixed input voltage, SS topology behaves as a constant current source, making it ideal for charging Li-ion or Li-polymer batteries. Therefore, the SS compensation topology was chosen for the charger design.

TABLE I
PARAMETERS OF THE CHARGER-IDEAL VALUES

Parameters	Values
Input voltage, V_{dc}	24 V
CV mode voltage, $V_{Batt,max}$	21 V
CC mode current, I_{Batt}	5 A
Minimum output voltage, $V_{Batt,min}$	12.6 V
Maximum output power, P_{out}	105 W
Switching frequency, f_{sw}	85 kHz
Primary inductance, L_{Tx}	33.30 μH
Secondary inductance, L_{Rx}	39.73 μH
Primary capacitance for 85kHz, C_{Tx}	105.27 nF
Secondary capacitance for 85kHz, C_{Rx}	88.23 nF
Nominal value of magnetic coupling	0.20
Range of magnetic coupling	0.1– 0.2
Maximum value of coil currents, I_{Tx} and I_{Rx}	10 A (RMS)

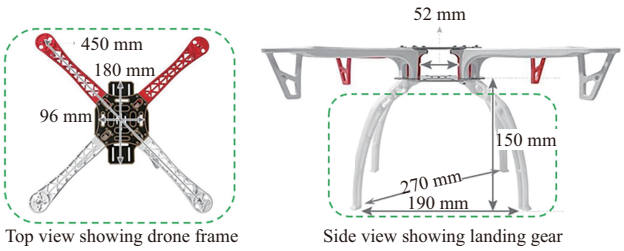

Fig. 3. Picture of F450 / Q450 quadcopter drone frame.

The rest of the paper is structured as follows: Section II covers the specifications of the coils and pads, along with key definitions used in this study. Section III presents the interoperability analysis, incorporating finite element analysis (FEA), hardware results, and the power transfer performance of the optimal Tx-Rx pairs. Finally, Section IV concludes the paper and outlines future work.

II. Coil and Pad Design: Specifications and Key Definitions

Various types of UAVs are commercially available, differing in frame shape, size, and landing gear. For this charger implementation, the F450 / Q450 quadcopter drone frame was selected due to its availability in the lab and widespread use in academia for research, owing to its versatility and low cost. Fig. 3 illustrates the drone frame, including its landing gear and key dimensions. Since the Rx coil must be mounted on the drone, its design is constrained by the height of the landing gear, which determines the clearance between the drone and the charging base. Additionally, the spacing between the landing gear defines the maximum allowable dimensions for the coil. In addition, Rx coil should remain within the drone's footprint to ensure efficient landing and charging without occupying excessive space on the charging platform.

TABLE II
COIL (RX) SPECIFICATIONS

Coil type	Outer size/mm	No. of turns	Overlap length/mm
BP 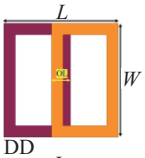	180 × 180 (*L*×*W*)	9 each	30
DD 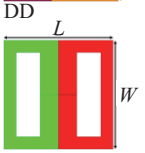	180 × 180 (*L*×*W*)	10 each	–
Circular 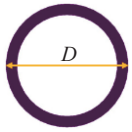	225 (*D*)	10	–

Keeping these constraints in mind, Rx coils of different shapes were designed, each with an inductance value equal to L_{Rx} as specified in Table I. As the Rx coil is typically mounted on the drone's landing gear, minimizing its weight is essential. This excludes the use of ferrite and aluminum backplates for shielding, as they would introduce unnecessary mass. The unshielded Rx coils are simply referred to as "coils" in this paper. In contrast, the Tx coil, installed at the charging base station, is not subject to weight limitations and can be designed for optimal flux generation across a designated charging zone, accommodating drones of various shapes and sizes. To minimize magnetic leakage, the Tx coil was shielded using a conventional ferrite and aluminum backplate configuration, collectively referred to as "pads" in this paper.

Three planar coil shapes were evaluated: circular, double-D (DD) [21]–[23], and bipolar (BP) [24]. The double-D quadrature (DD-Q) coil exhibits similar magnetic characteristics to the BP coil but requires more copper, therefore, it was not considered for implementation. The design and analysis of both Tx and Rx coils were conducted using Ansys Maxwell [25]. To minimize high-frequency losses and meet the charger's current requirements, 16AWG Litz wire of specification 420/42 SPN SN (420 strand, 42 AWG each strand) was used. Shielding was implemented using 54 mm×14 mm×5 mm I-type ferrite blocks made of CF297 material from COSMO ferrites, with an aluminum backplate. The dimensions of all coils and pads designed in the Ansys are summarized in Tables II and III, respectively.

Magnetic flux generated by coil or pad can be decomposed into perpendicular and parallel components. The relative dominance of these components determines the interoperability among coils or pads. For instance, if a coil or pad predominantly generates a perpendicular flux component, it can only couple effectively with other coils producing a similar flux orientation. Conversely, it will not be interoperable with coils that primarily generate a parallel flux component. The definitions of parallel and perpendicular flux components are illustrated in Fig. 4 and will be referenced throughout this paper.

The flux pattern generated by a coil depends not only on its geometry but also on its excitation mode. Single-coil structures typically generate a fixed flux pattern. For example, in a circular pad (CP) or coil, the perpendicular flux component is dominant. However, multi-coil structures, such as the bipolar pad (BPP) or coil, can produce both perpendicular and parallel flux components depending on the excitation mode.

The excitation mode plays a crucial role in the performance and interoperability of multi-coil structures such as double-D pad (DDP) and BPP. While CP and DDP coils have only two terminals, the BP coil features four terminals, allowing for multiple excitation modes. For interoperability analysis, the DDP was examined in its conventional configuration, where both coils are magnetically in series and electrically in parallel, resulting in two accessible terminals. In contrast, the BPP supports independent excitation of each coil through its four-terminal design [26]. When used as a Tx pad, each coil of the BPP can be excited using separate inverters. However, to simplify the system and reduce costs, the excitation scheme for this study was limited to two accessible terminals, allowing the use of a single inverter.

Using a single inverter, the BP coil can operate in two distinct excitation modes, namely 0° excitation mode and 180° excitation mode. In the 0° excitation mode, the currents in both coils flow in-phase, either clockwise (CW) or counterclockwise (CCW) as shown in Fig. 5(a). In the 180° excitation mode, the currents flow in opposite directions (CW in one coil and CCW in the other), as illustrated in Fig. 5(b). The flux orientation depends on the excitation mode: The 0° excitation mode generates a perpendicular flux component, while the 180° excitation mode produces a parallel flux component. This behavior is validated through simulations in Ansys Maxwell.

Fig. 6(a) and (b) shows the flux patterns generated by the BP pad in the 0° and 180° excitation modes, respectively, with black dotted lines indicating the dominant field pattern. These patterns were compared with the flux distributions of the CP and the DDP. As observed, the BPP in the 0° excitation mode produces a non-polarized perpendicular flux pattern similar to the CP as shown in Fig. 6(c). However, unlike the CP, the flux magnitude is not perfectly symmetric around the pad's center due to the geometric asymmetry between its two coils. On the other hand, the BPP in the 180° excitation mode generates a polarized parallel flux pattern along the pad's length, closely resembling the flux distribution of the DDP as shown in Fig. 6(d).

III. DESIGN VALIDATION AND HARDWARE IMPLEMENTATION

A. Coil and Pad Fabrication and Inductance Values

The self-inductance and equivalent series resistance (ESR) of the coils and pads were measured using the HAMEG HM8118 Programmable LCR meter and compared with simulation results from Ansys Maxwell. The findings from

TABLE III
PAD (TX) SPECIFICATIONS

Pad type	Outer size of coils/mm	No. of turns	Overlap length/mm	Shield (Aluminum, polycarbonate holder)/mm
BPP 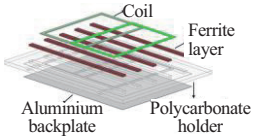	300 × 250	5 each	54	400×280×0.7, 480×360×10
DDP 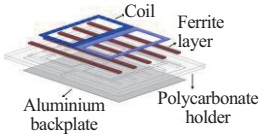	300 × 250	5 each	–	400×280×0.7, 480×360×10
CP 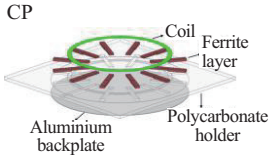	308 (diameter)	6	–	400(diameter), 480×480×10

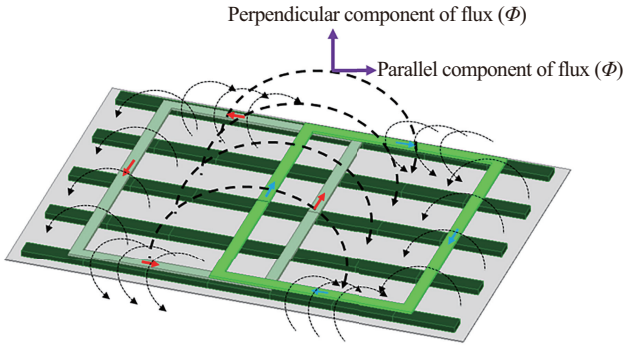

Fig. 4. Parallel and perpendicular components of flux generated by BPP in 180° excitation mode.

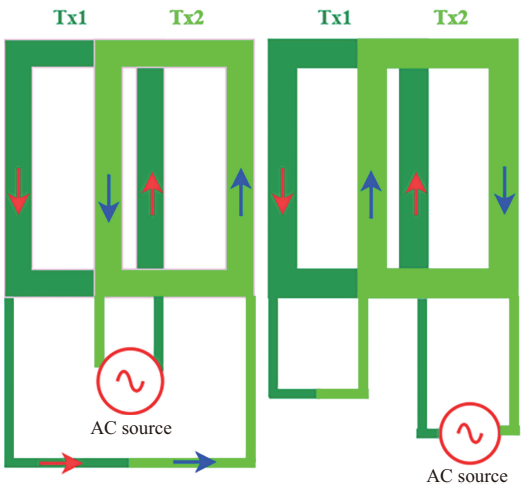

Fig. 5. BP coil in (a) 0° excitation mode and (b) 180° excitation mode.

both simulation and hardware measurements are summarized in Tables IV and V.

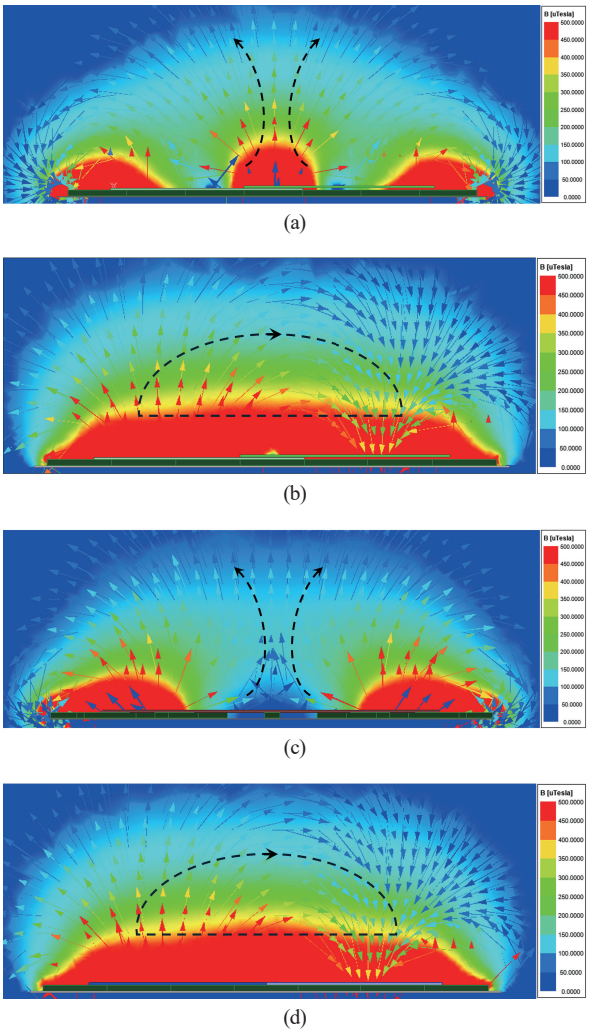

Fig. 6. Magnetic flux density (B) generated by (a) BPP (0° excitation mode), (b) BPP (180° excitation mode), (c) CP, and (d) DDP.

TABLE IV
INDUCTANCE AND ESR VALUES FOR FABRICATED RX COILS

Coil type		Inductance L_{Rx}/μH		ESR R_{Rx}/mΩ	
		Simulation	Hardware	Simulation	Hardware
BP 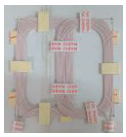	BP: (0° Mode)	37.83	39.89	129.47	113.87
	BP: (180° Mode)	42.72	44.10	128.82	111.64
DD 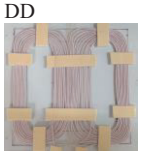		40.69	41.09	164.46	96.259
Circular 		40.56	41.47	94.87	109.34

TABLE V
INDUCTANCE AND ESR VALUES FOR FABRICATED TX PADS

Pad type		Inductance L_{Tx}/μH		ESR R_{Tx}/mΩ	
		Simulation	Hardware	Simulation	Hardware
BPP 	BPP (0° mode)	36.63	38.46	148.62	169.54
	BPP (180° mode)	36.36	38.03	136.37	148.94
DDP 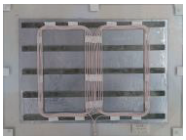		34.36	33.05	174.87	120.66
CP 		31.62	30.42	114.82	116.14

Multiple design iterations were performed to match the ideal inductance values from Table I, but some discrepancies remained. These variations between simulation and hardware results stemmed from challenges in maintaining ideal inter-turn spacing, as well as exact length and width, as modeled in the simulation.

B. Interoperability Analysis and Results

Power transfer between the Tx and Rx coils relies on magnetic coupling, making the coupling coefficient (*k)* a key metric for assessing the interoperability of different Tx-Rx pairs. This analysis evaluates variations in "*k*" across air gaps ranging from 10mm to 100mm and misalignments in the *x* and *y* directions from −250 mm to 250 mm, covering the entire charging zone. The charging zone is defined based on the landing gear footprint, while the air gap is determined by the landing gear height. As shown in Fig. 3, the leg spacing varies along the height of the landing gear; therefore, a maximum air gap of 100 mm is considered for coupling evaluation. During misalignment evaluations for each Tx-Rx pair, the air gap is fixed at 60 mm. The coordinate system used for simulations and hardware measurements is illustrated in Fig. 7(a). An example of y-direction misalignment and the hardware setup

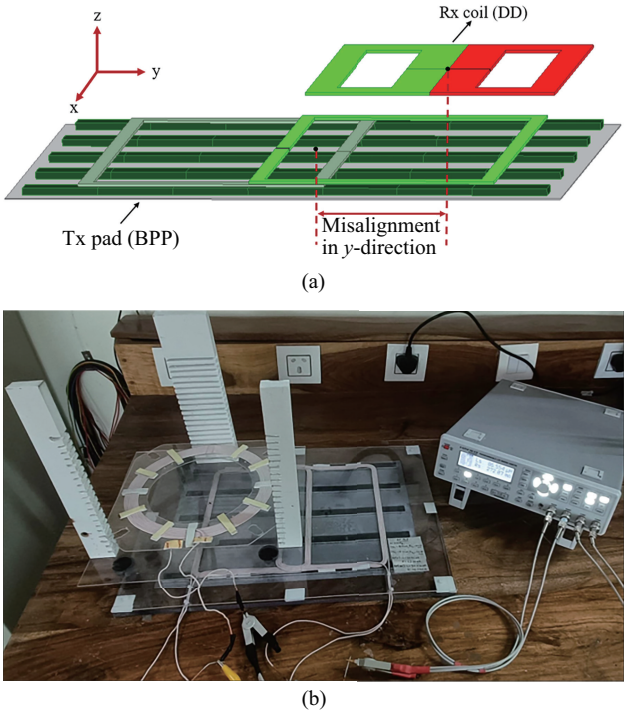

Fig. 7. Misalignment analysis. (a) Coordinate system and *y*-direction misalignment between Tx pad and Rx coil. (b) Experimental hardware setup for misalignment measurements.

TABLE VI
VARIOUS TX-RX COMBINATIONS USED FOR INTEROPERABILITY ANALYSIS

Pad-coil combinations	
Tx	Rx
BPP (0° mode)	• Circular coil • DD coil • BP (180° mode) coil • BP (0° mode) coil
BPP (180° mode)	• Circular coil • DD coil • BP (180° mode) coil • BP (0° mode) coil
DDP	• Circular coil • DD coil • BP (180° mode) coil • BP (0° mode) coil
CP	• Circular coil • DD coil • BP (180° mode) coil • BP (0° mode) coil

for misalignment analysis is shown in Fig. 7(b). The various Tx-Rx combinations used in this study are summarized in Table VI.

1) BPP (0° mode) as Tx: In this excitation mode, BPP generates a non-polarized perpendicular flux pattern. Since DD and BP (180°) receivers primarily couple with parallel flux, their interoperability is inherently weak. Simulations and hardware measurements confirm this, showing no coupling with *x*-misalignment and only minimal, yet insufficient, coupling with *y*-misalignment. However, it was interoperable with both

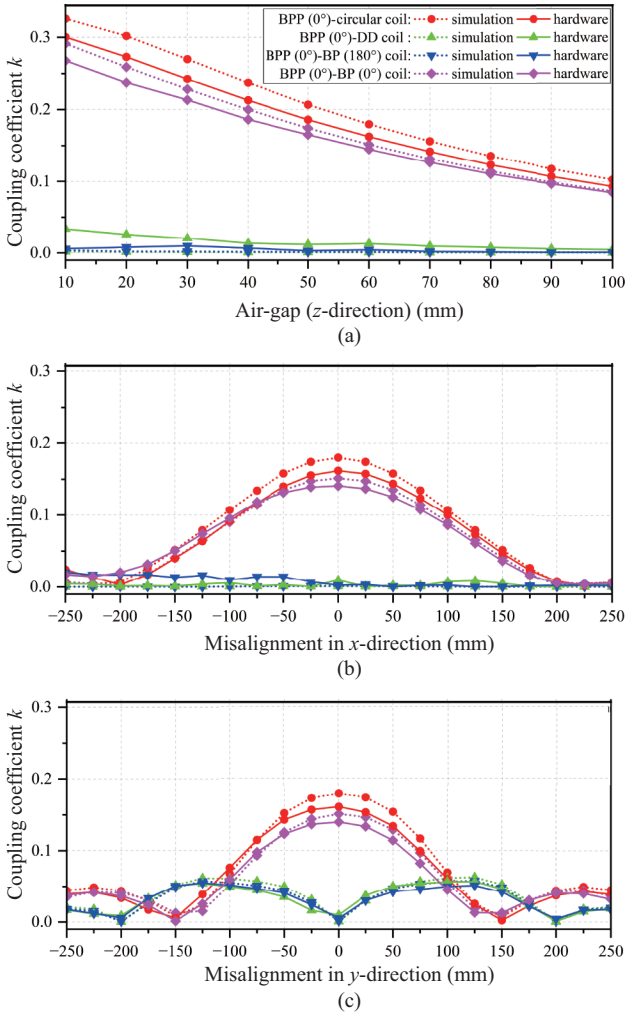

Fig. 8. Coupling performance with BPP (0° mode) as Tx.Variation of *k* with (a) airgap, (b) *x*-misalignment, and (c) *y*-misalignment.

circular and BP (0°) receivers, demonstrating similar tolerance to misalignment in both *x* and *y* directions, with magnetic nulls occurring around ±200 mm for *x*-misalignment and ±150 mm for *y*-misalignment. The variation of *k* with air gap, *x*- and *y*-misalignment is shown in Fig. 8.

2) BPP (180° mode) as Tx: In 180° excitation mode, the BP coil generates a parallel flux pattern similar to that of the DDP, with magnetic null points occurring around ±75 mm along the *y*-direction misalignment for both BP (180°) and DD receivers. Circular and BP (0°) receivers exhibited the weakest coupling, as they primarily interact with perpendicular flux components. No coupling was observed with *x*-misalignment, while significant improvements in coupling were noted along the *y*-direction misalignment, except in the perfectly aligned condition. The variations in coupling with air gap, *x*- and *y*-misalignment are shown in Fig. 9.

3) DDP as Tx: For the DDP, significant improvements in coupling were observed only along the *y*-misalignment for circular and BP (0°) receivers, while no interoperability was observed under *x*-misalignment. Fig. 10 illustrates the variation of *k* with air gap, *x*- and *y*-misalignment.

4) CP as Tx: DD and BP (180°) receivers showed the weakest

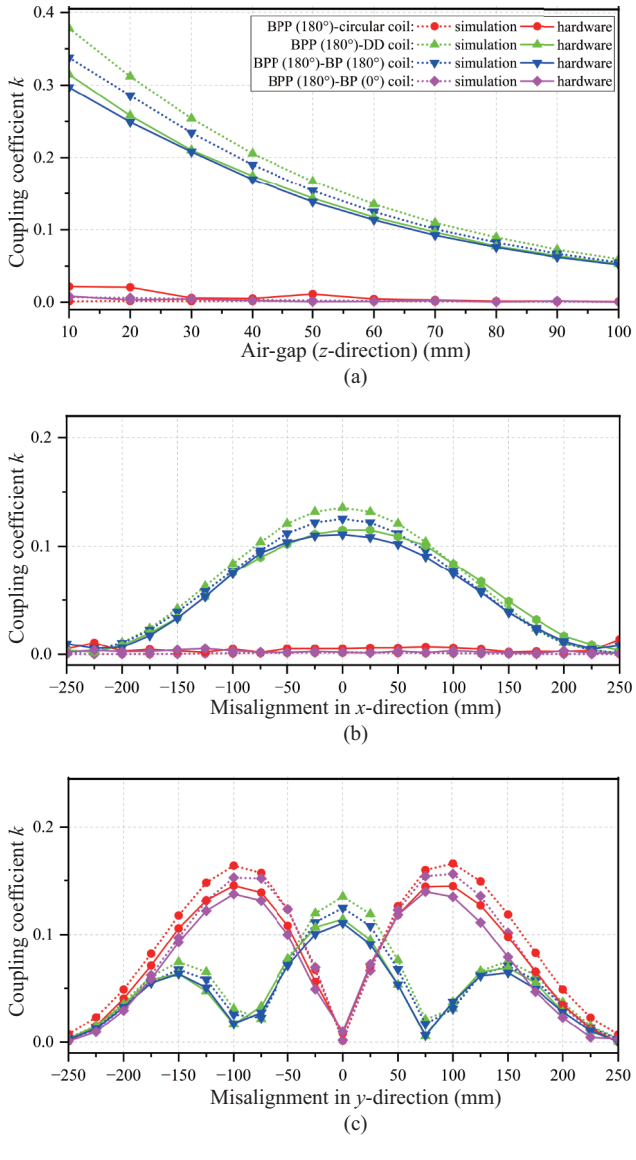

Fig. 9. Coupling performance with BPP (180°mode) as Tx. Variation of k with (a) airgap, (b) x-misalignment, and (c) y-misalignment.

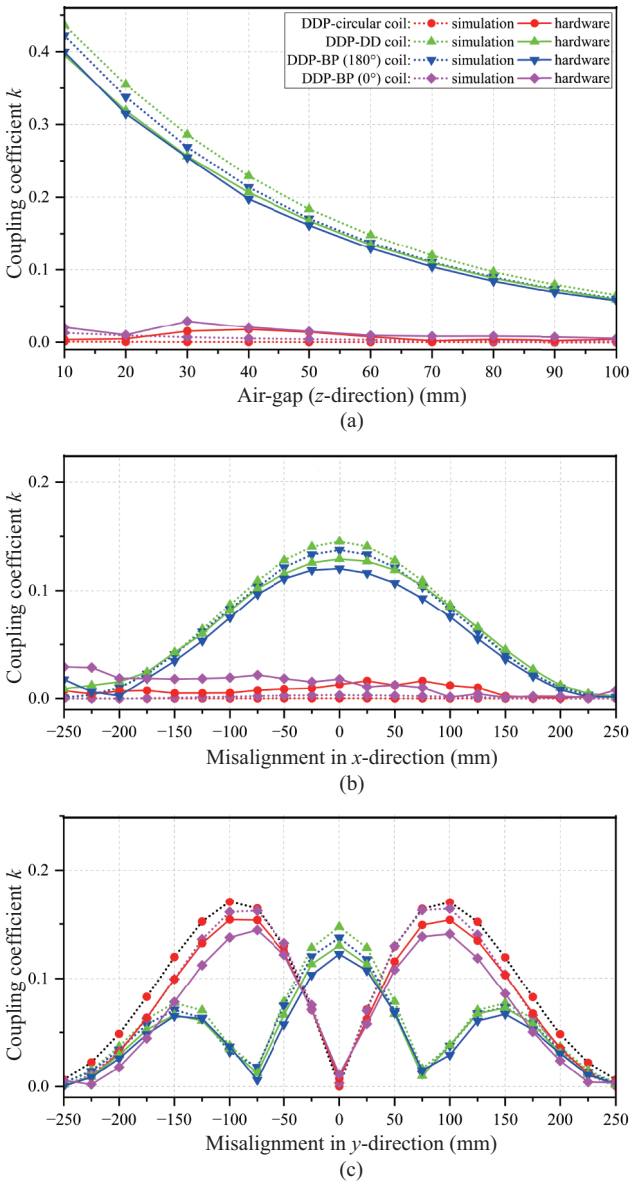

Fig. 10. Coupling performance with DPP as Tx. Variation of k with (a) airgap, (b) x-misalignment, and (c) y-misalignment

coupling, with negligible improvements in k values along y-misalignment. BP (0°) demonstrated the best misalignment tolerance in both directions but had lower coupling compared to the circular receiver. Fig. 11 illustrates the variation of the coupling factor with air gap, x- and y-misalignment.

Several key insights were gained from the analysis of interoperable Tx-Rx pairs, as summarized in Table VII. Since the nominal coupling for the charger is 0.2, as specified in Table I, further analysis was conducted to determine the required air gap for 0.2 coupling between the Tx and Rx coils for practical implementation. Additionally, the impact of lateral misalignment on coupling performance was examined at nominal air-gap, which is discussed in the next section.

C. Selection of Best Tx-Rx Pair and Power Transfer Performance

The interoperability analysis identified the strengths and limitations of each Tx-Rx combination in terms of coupling variations with airgap and lateral misalignment. Since the Rx coil is fixed on the drone, the airgap remains constant and is not a concern. However, coupling variations due to x or y misalignment must still be addressed. For example, a DD/BP (180°) receiver paired with a DDP/BPP (180°) Tx exhibits different coupling behaviors in both directions and encounters magnetic nulls, significantly reducing the charging zone.

These insights guided the selection of the most suitable Tx-Rx pairs. Given the similar magnetic characteristics of circular and BP (0°) coils, the choice was narrowed to these receivers. The final selection was based on three key criteria: the airgap required for nominal coupling ($k \approx 0.2$), coupling variation due to misalignment, and the position of magnetic null points. For this purpose, Tx-Rx pairs were simulated to obtain the airgap for a coupling of 0.2. Using the same air-gap, their misalignment performance was assessed in simulation, and the resonant link efficiency of the interoperable Tx-Rx pairs were calculated using (1) [27]. The results are illustrated in Fig. 12

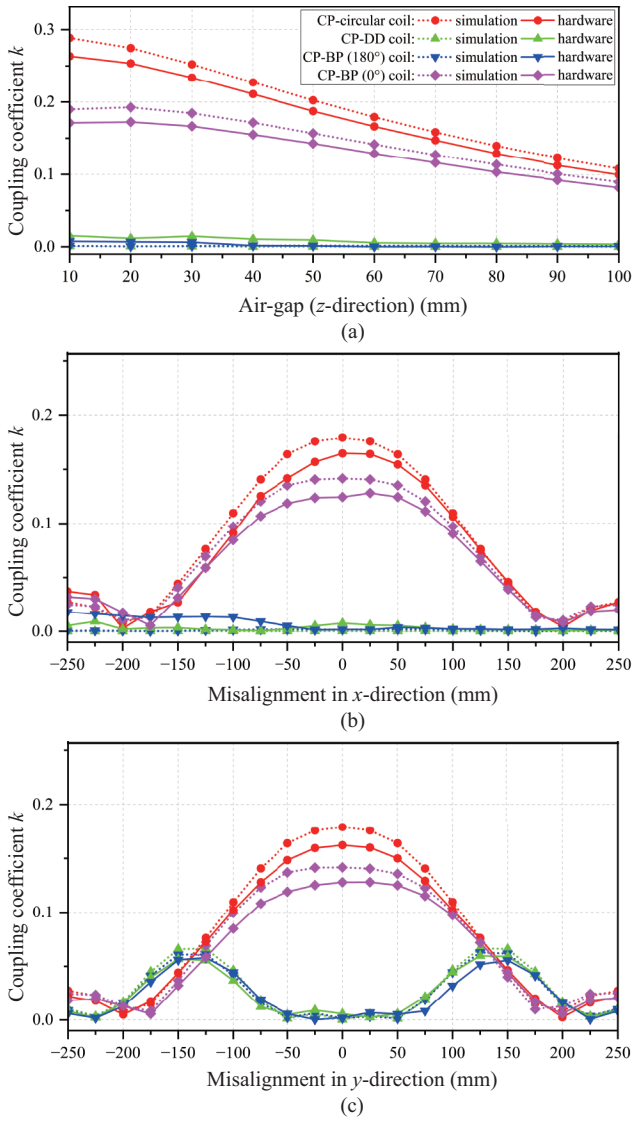

Fig. 11. Coupling performance with CP as Tx. Variation of k with (a) airgap, (b) x-misalignment, and (c) y-misalignment.

and summarized in Tables VIII and IX.

$$\eta = \frac{R_L}{(R_{\mathrm{Rx}} + R_L)\left(1 + \dfrac{R_{\mathrm{Tx}}R_{\mathrm{Rx}} + R_{\mathrm{Tx}}R_L}{M^2\omega_0^2}\right)} \tag{1}$$

While the CP-BP (0°) pair demonstrated superior misalignment tolerance (±75mm in both x and y directions), and high resonant-link efficiency under both aligned and misaligned conditions, the air-gap is only 20 mm for nominal coupling as shown in Tables VIII and IX. Such a small air-gap is less desirable for practical UAV charging applications. Furthermore, at this reduced air-gap, the receiver inductance is significantly influenced by Tx-side shielding, leading to variations in resonant tuning. Similarly, the BPP (0°)-BP (0°) pair, though offering balanced misalignment performance, exhibited increased sensitivity to airgap variations due to Tx shielding effects, causing the changes in magnetic nulls position. The

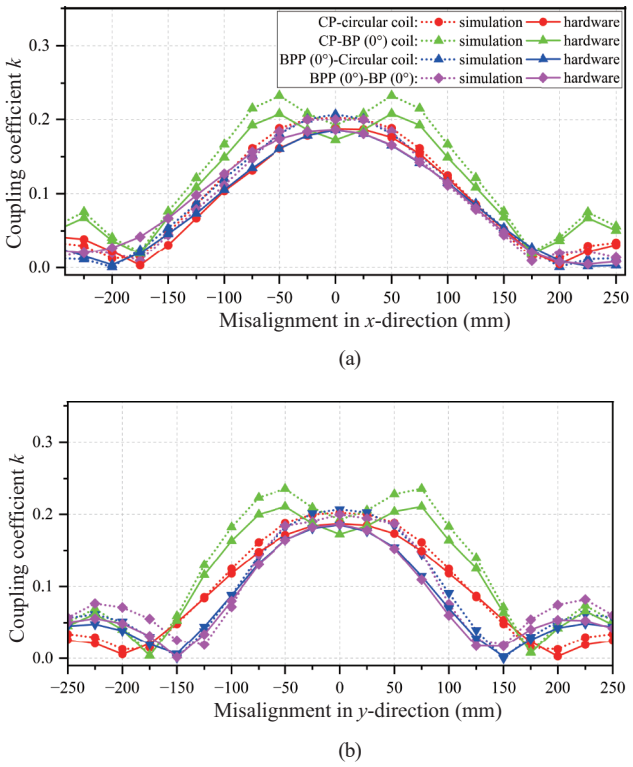

Fig. 12. Variation of k with x-misalignment and air-gap fixed to have 0.2 coupling in perfect alignment for each pair. (a) x-misalignment. (b) y-misalignment.

BPP (0°)-circular pair had the lowest misalignment tolerance (±25 mm), further limiting its suitability.

With a well-balanced misalignment tolerance (±50 mm in both x and y directions), magnetic nulls positioned at ±200 mm, and consistently high resonant-link efficiency under both aligned and misaligned conditions, the CP-circular pair offers the best trade-off between coupling stability, airgap clearance, misalignment robustness, and energy transfer efficiency. Therefore, it was chosen to implement the charger.

The circular Rx was mounted on the drone frame and tested for power transfer capabilities in perfect alignment, 50 mm misalignment, and 100 mm misalignment, all with an air gap of 50 mm. For testing the Tx-Rx coil pair, an inverter was built using TK22E10N1 MOSFETs (Toshiba) and IR2110 gate drivers (Infineon), while a rectifier was implemented with 12TQ100 Schottky diodes (SMC Diode Solutions). PWM pulses were generated by a TMS320F28379D microcontroller evaluation board (Texas Instruments). As this study focuses on coil design, readily available components were used for the inverter and rectifier to validate power transfer capability. However, the final design will incorporate optimized components, such as an SMD-based rectifier for compact integration. An IT8514C electronic load (ITECH) was used to apply the load on the charger, and an M3904C-500-24 DC power supply (ITECH) powered the inverter.

The values of the compensation capacitors and switching frequency used in the hardware setup differ slightly from the ideal values listed in Table I. This deviation was necessary

TABLE VII
PERFORMANCE SUMMARY OF TX-RX PAIRS

Tx	Rx	k at 100 mm airgap (Perfect alignment)	Magnetic null (x-Misalignment)/mm	Magnetic null (y-Misalignment)/mm	Interoperable
BPP (0°)	Circular	0.1	±200	±150	Yes
	DD	0	-	0, ±200	No
	BP (180°)	0	-	0, ±200	No
	BP (0°)	0.08	±200	±150	Yes
BPP (180°)	Circular	0	-	0	Only along y-direction
	DD	0.05	±225	±75	Yes
	BP (180°)	0.05	±225	±75	Yes
	BP (0°)	0	-	0	Only along y-direction
DDP	Circular	0	-	0	Only along y-direction
	DD	0.06	±225	±75	Yes
	BP (180°)	0.06	±225	±75	Yes
	BP (0°)	0	-	0	Only along y-direction
CP	Circular	0.1	±200	±200	Yes
	DD	0	-	0 to ±50, ±225	No
	BP (180°)	0	-	0 to ±50, ±225	No
	BP (0°)	0.09	±200	±175	Yes

TABLE VIII
PERFORMANCE SUMMARY OF MOST SUITABLE TX-RX PAIRS
mm

Tx-Rx pairs	Airgap for $k \approx 0.2$	x-misalignment tolerance	y-misalignment tolerance	Magnetic null (x, y)
CP-circular	50	±50	±50	±200, ±200
CP- BP (0°)	20	±75	±75	±175, ±175
BPP (0°)-Circular	50	±25	±25	±200, ±150
BPP (0°)- BP (0°)	40	±50	±50	±175, ±125

TABLE IX
RESONANT LINK EFFICIENCY EVALUATION OF THE INTEROPERABLE TX-RX PAIRS
%

Interoperable Tx-Rx pairs	Efficiency at 0 mm misalignment	Efficiency at 50 mm y - misalignment	Efficiency at 100 mm y - misalignment)
CP-circular	94.37	93.90	89.55
CP- BP (0°)	93.14	94.51	93.04
BPP (0°)-circular	93.94	92.85	76.30
BPP (0°)- BP (0°)	93.41	92.27	67.43

to accommodate the difference between the inductance of the fabricated coil and the ideal inductance, as well as due to the practical availability of components in the market. The parameters of the hardware setup are summarized in Table X. The hardware setup is shown in Fig. 13, with results for perfect alignment presented in Fig. 14, for 50 mm misalignment in Fig. 15, and for 100 mm misalignment in Fig. 16.

From Fig. 14, the system operates as expected under perfect alignment, delivering a stable 21V output voltage and 5 A load current. Since the system is tolerant up to ±50 mm, only a slight reduction in output voltage and current can be observed, as shown in Fig. 15(b). However, under 100 mm misalignment, the Tx and receiver coil currents increase, as shown in Fig. 16(a). With a fixed load, this results in a higher output voltage, highlighting the need for a closed-loop controller, which will be addressed in future work. Notably, even with a 100 mm

TABLE X
PARAMETERS OF THE HARDWARE SETUP

Parameters	Value
L_{Tx}	30.42 µH
L_{Rx}	41.47 µH
C_{Tx}	98.04 nF
C_{Rx}	79.6 nF
f_{sw}	90 kHz
V_{dc}	24 V
Load resistance (R_L)	4.2 Ω

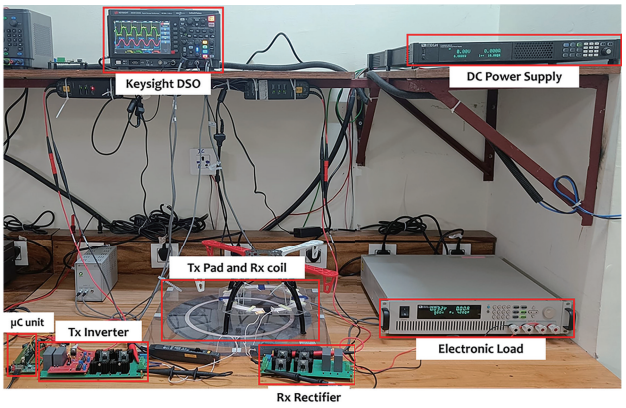

Fig. 13. Hardware setup.

misalignment, the maximum current remains below 10 A RMS, well within the current-handling capacity of the Litz wire used in the coil fabrication. Table XI summarizes the charging efficiency under different misalignment conditions. It can be observed that under perfect coupling, the efficiency is 86.77%, with only a slight reduction at a 50 mm misalignment. Beyond the tolerance zone, the efficiency decreases to 81.5%, representing a significant drop compared to the perfectly aligned condition.

IV. CONCLUSION AND FUTURE WORK

This paper conducted a comprehensive interoperability analysis of various Tx pad-Rx coil pairs to identify the most effective configuration for UAV wireless charging. The evaluation considered coupling performance across different airgaps and misalignment conditions, leading to key insights into the strengths and limitations of each pairing.

The CP-circular coil pair emerged as the most suitable choice, offering the largest airgap while maintaining stable coupling and consistent misalignment tolerance in both x and y directions. Other configurations, such as CP-BP (0°) and BPP (0°)-circular, demonstrated promising performance but were constrained by increased sensitivity to airgap variations or reduced misalignment tolerance, ultimately limiting their practical application. Poorly performing pairs exhibited significant coupling fluctuations, with some failing to achieve

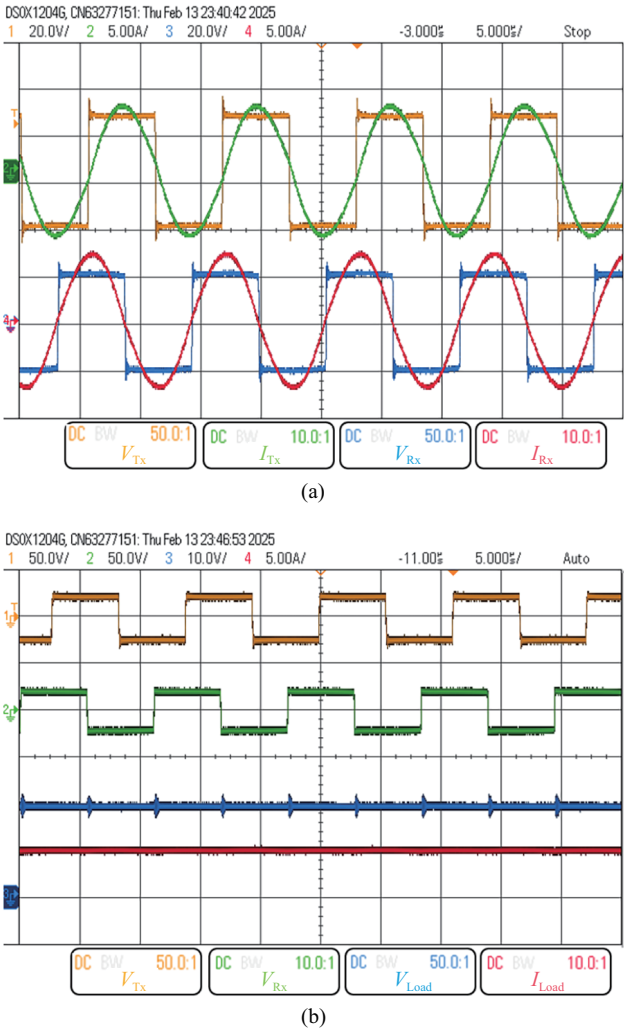

Fig. 14. Charger waveforms at air-gap of 50 mm (k = 0.2) and 0 misalignment. (a) Tx and Rx side voltage and current. (b) Tx and Rx side voltage and load side voltage and current.

stable power transfer under misalignment.

By selecting the CP-circular combination, this work ensures a more robust and efficient charging solution, allowing UAVs to dock from multiple directions without compromising performance. Experimental validation confirmed the system's effectiveness, aligning with the intended design objectives.

Future research will focus on enhancing system efficiency through closed-loop control for Li-ion battery charging. Further developments will also explore advanced features, including coil detection and metal object detection (MOD), to improve reliability and safety in real-world applications.

REFERENCES

[1] T. Feng, K. Shi, J. Jiang, and P. Wang, "A solenoid magnetic coupler and its control method for omnidirectional wireless charging of UAVs," in *IEEE Transactions on Industrial Electronics*, vol. 72, no. 3, pp. 2540–2550, Mar. 2025.

[2] Y. Zhao, S. Shen, F. Yin, and L. Wang, "A high misalignment-tolerant hybrid coupler for unmanned aerial vehicle WPT charging systems," in *IEEE Transactions on Transportation Electrification*, vol. 11, no. 1, pp. 1570–1581, Feb. 2025.

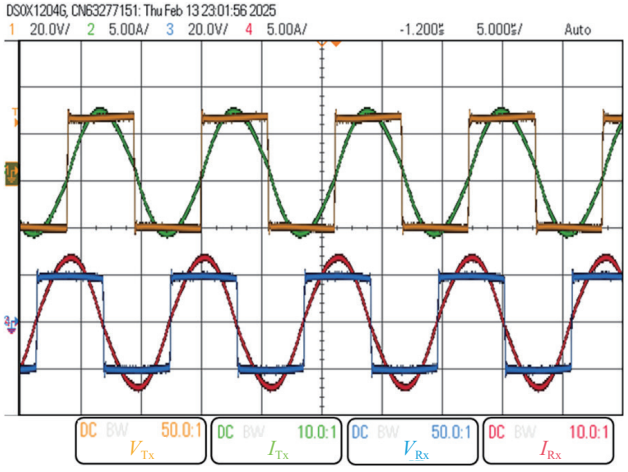

(a)

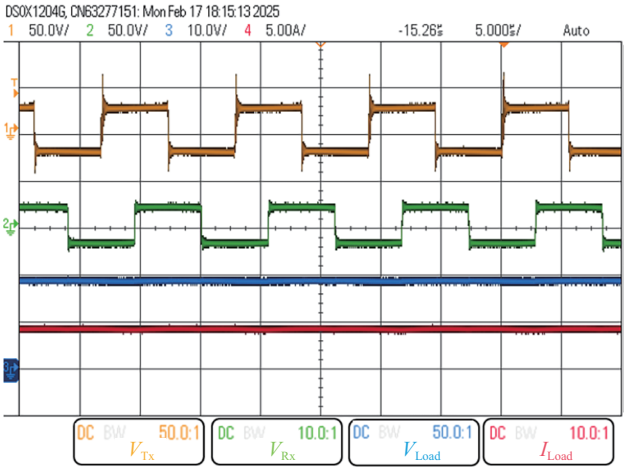

(b)

Fig. 15. Charger waveforms at air-gap of 50 mm and misalignment of 50 mm. (a) Tx and Rx side voltage and current. (b) Tx and Rx side voltage and load side voltage and current.

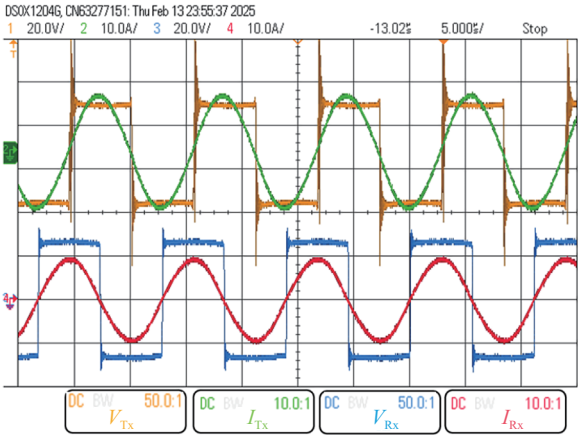

(a)

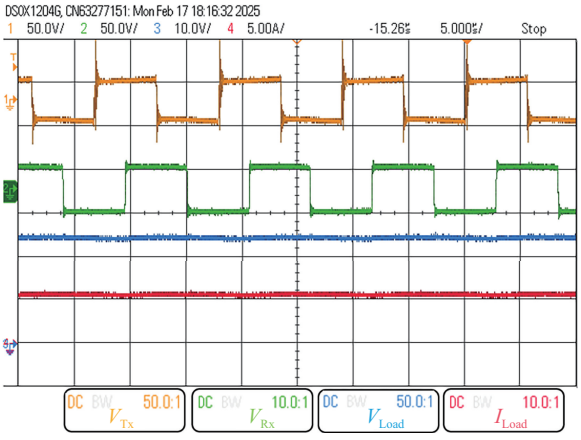

(b)

Fig. 16. Charger waveforms at air-gap of 50 mm and misalignment of 100 mm. (a) Tx and Rx side voltage and current. (b) Tx and Rx side voltage and load side voltage and current.

TABLE XI
EFFICIENCY COMPARISON OF CP-CIRCULAR PAIR

Misalignment/mm	Efficiency/%
0	86.77
50	85.75
100	81.5

[3] Y. Guan, Y. Qiao, J. Mai, Y. Wang, and D. Xu, "Compensation parameter optimization of inductive wireless power transfer system for low stray magnetic field," in *IEEE Trans Power Electron*, vol. 40, no. 5, pp. 7537–7548, May 2025.

[4] S. Wu, C. Cai, H. Zhang, X. Liu, and W. Chai, "A free-positioning IPT system via reconfigurable coil array transmitter for unmanned aerial vehicle applications," in *IEEE Transactions on Transportation Electrification*, vol. 10, no. 4, pp. 8746–8757, Dec. 2024.

[5] X. Mou, D. Gladwin, J. Jiang, K. Li, and Z. Yang, "Near-field wireless power transfer technology for unmanned aerial vehicles: A systematical review," in *IEEE Journal of Emerging and Selected Topics in Industrial Electronics*, vol. 4, no. 1, pp. 147–158, Nov. 2022.

[6] Y. Zhang, C. Liu, M. Zhou, and X. Mao, "A novel asymmetrical quadrupolar coil for interoperability of unipolar, bipolar, and quadrupolar coils in electric vehicle wireless charging systems," in *IEEE Transactions on Industrial Electronics*, vol. 71, no. 4, pp. 4300–4303, Apr. 2024.

[7] C. Liu, M. Zhou, R. Xie, Y. Zhuang, and Y. Zhang, "Study on interoperability and misalignment tolerance of electric vehicle wireless charging system based on a novel asymmetrical bipolar coil," in *IEEE Access*, vol. 12, pp. 104920–104927, 2024.

[8] Y. Zhang, W. Pan, C. Liu, Z. Shen, Y. Wu, Y. Zhang, and Z. Li, "Interoperability study of electric vehicle wireless charging system based on three decoupled nonoverlapping unipolar transmitting coils," in *IEEE Transactions on Transportation Electrification*, vol. 10, no. 4, pp. 8630–8639, Dec. 2024.

[9] M. M. Rahman, M. S. I. Shanto, N. Sarker, T. Rani, and L. C. Paul, "A comprehensive review of wireless power transfer methods, applications, and challenges," in *Engineering Reports*, vol. 6, no. 10, pp. 2577–8196, Oct. 2024.

[10] S. Yoon, T. Lim, and Y. Lee, "Multifunctional coil technique for alignment-agnostic and Rx coil size-insensitive efficiency enhancement for wireless power transfer applications," in *Scientific Reports*, vol. 13, no. 1, Dec. 2023.

[11] M. Machnoor, E. S. Gamez Rodriguez, P. Kosta, J. Stang, and G. Lazzi, "Analysis and design of a 3-coil wireless power transmission system for biomedical applications," in *IEEE Transactions on Antennas and Propagation*, vol. 67, no. 8, pp. 5012–5024, Aug. 2019.

[12] B. Zhang, J. Deng, M. Duan, C. Li, Y. Zheng, S. Wang, "Design and implementation of interoperable high-efficiency bidirectional wireless power transfer systems for multiple vehicles," in *Green Energy and Intelligent Transportation*, no.2, p. 100307, Mar. 2025.

[13] K. Aditya, "Sizing wireless battery charger for the CC-CV charging of lithium polymer battery used in unmanned aerial vehicle," in

Proceedings of 2023 IEEE 3rd International Conference on Sustainable Energy and Future Electric Transportation(SEFET), Bhubaneswar, India, 2023, pp. 1–6.

[14] A. Mahesh, B. Chokkalingam, R. Verma, and L. Mihet-Popa, "Load invariant CC and CV modes for static/dynamic wireless charging system with half-bridge multi-leg converter topology," in *IEEE Access*, vol. 13, pp. 9654–9665, 2025.

[15] Y. Zhang, H. Tang, Z. Shen, Y. Zhuang, and Z. Li, "An LC squared-compensated inductive power transfer system with misalignment tolerance and constant-current output," in *IEEE Trans Power Electron*, vol. 39, no. 4, pp. 4850–4857, Apr. 2024.

[16] Y. Fei, F. Chen, R. Gao, S. Zhao, C. Tang, and L. Zhao, "Oscillation frequency manipulation in autonomous WPT systems with series-series compensation," in *IEEE Transactions on Power Electronics*, vol. 39, no. 1, pp. 58–63, Jan. 2024.

[17] X. Liu, F. Gao, H. Niu, G. Sun, T. Wang, and H. Wang, "A series-parallel transformer-based WPT system for 400-V and 800-V electric vehicles with Z1 or Z2 class," in *IEEE Transactions on Power Electronics*, vol. 39, no. 1, pp. 1749–1761, Jan. 2024.

[18] S. Ren, X. Wang, J. Xu, and P. Yang, "Primary-side resonant current/voltage clamped IPT systems without clamping coil or isolation transformer for inherent CC-to-CV charging," in *IEEE Journal of Emerging and Selected Topics in Power Electronics*, vol. 13, no. 1, pp. 1281–1294, Feb. 2025.

[19] K. Aditya and S. S. Williamson, "Design guidelines to avoid bifurcation in a series-series compensated inductive power transfer system," in *IEEE Transactions on Industrial Electronics*, vol. 66, no. 5, pp. 3973–3982, May 2019.

[20] Y. Mao, Y. Yang, and K. Wang, "A primary-side fixed-frequency CC and CV output control for single-stage wireless battery chargers with series compensation receivers," in *IEEE Transactions on Transportation Electrification*, vol. 10, no. 2, pp. 3407–3415, Jun. 2024.

[21] U. Gordhan and S. Jayalath, "Comparative analysis of wireless power transfer couplers for unmanned aerial vehicles and drones," in *IEEE Open Journal of Power Electronics*, vol. 5, pp. 618–633, 2024.

[22] C. Cai, D. Shen, S. Wu, X. Liu, and W. Chai, "A high misalignment tolerance IPT system for unmanned aerial vehicles based on multi-winding combined coupling," in *IEEE Transactions on Transportation Electrification*, vol. 10, no. 4, pp. 8566–8574, Dec. 2024.

[23] M. Budhia, J. T. Boys, G. A. Covic, and C. Y. Huang, "Development of a single-sided flux magnetic coupler for electric vehicle IPT charging systems," in *IEEE Transactions on Industrial Electronics*, vol. 60, no. 1, pp. 318–328, 2013.

[24] A. Zaheer, G. A. Covic, and D. Kacprzak, "A bipolar pad in a 10-kHz 300-W distributed IPT system for AGV applications," in *IEEE Transactions on Industrial Electronics*, vol. 61, no. 7, pp. 3288–3301, 2014.

[25] ANSYS Inc., "ANSYS Electromagnetics Suite 2022 R1," 2022, *ANSYS Inc., Canonsburg, PA, USA*: 2022 R1. Accessed: Mar. 10, 2025. [Online]. Available: https://www.ansys.com

[26] A. Zaheer, H. Hao, G. A. Covic, and D. Kacprzak, "Investigation of multiple decoupled coil primary pad topologies in lumped IPT systems for interoperable electric vehicle charging," in *IEEE Transactions on Power Electronics*, vol. 30, no. 4, pp. 1937–1955, 2015.

[27] K. Aditya and S. S. Williamson, "A review of optimal conditions for achieving maximum power output and maximum efficiency for a series–series resonant inductive link," in *IEEE Transactions on Transportation Electrification*, vol. 3, no. 2, pp. 303–311, Jun. 2017.

Sushan Pradhan received the B.Tech. and M.Tech. degrees in Electrical Engineering from the Sikkim Manipal Institute of Technology, India, in 2018 and 2021, respectively. He is currently pursuing the Ph.D. degree with the Transportation Electrification Lab (T.E.L), Department of Electrical Engineering, IIT Jodhpur, India. His research interests include electric vehicles, wireless power transfer, coil design, finite element modelling, power electronics, wireless power transmission, and foreign object detection.

Avishek Munsi received the B.Sc. degree (Hons.) in physics and the B.Tech. and M.Tech. degrees (Hons.) in Electrical Engineering from the University of Calcutta, India, in 2015, 2018, and 2020, respectively. He is currently pursuing the Ph.D. degree with the Transportation Electrification Lab (T.E.L), Department of Electrical Engineering, IIT Jodhpur, India. His research interests include power converter design and control, wireless power transmission, and the development of advanced power electronics solutions for emerging applications.

Kunwar Aditya received the B.E. degree from Bharati Vidyapeeth University, Pune, India, in 2009, the M.Tech. degree from Indian Institute of Technology (Banaras Hindu University), Varanasi, India, in 2012, and the Ph.D. degree from the University of Ontario Institute of Technology (UOIT), Oshawa, ON, Canada, in 2016, all in electrical engineering. From July 2017 to November 2017, he was a Research Fellow with the Rolls-Royce@NTU Corporate Laboratory, Nanyang Technological University, Singapore. In December 2017, he joined BorgWarner Inc., Waterloo, ON, as a hardware engineer, where he contributed to the development of electric vehicle motor controllers for 800 V battery systems. In April 2019, he joined Vitesco Technologies Canada, Chatham, ON, as the technical project leader, focusing on the development and validation of sensors and actuators for electric vehicle thermal management systems. He is currently an Associate Professor with the Department of Electrical Engineering, Indian Institute of Technology (IIT) Jodhpur, India. At IIT Jodhpur, he leads research in power electronics, wireless charging, and energy storage systems, with emphasis on advancing sustainable transportation and renewable energy integration. His research interests include power conversion, linear control systems, and transportation electrification. Dr. Aditya was awarded the IIT (BHU) Gold Medal for securing the highest academic standing among all electrical engineering students of the 2012 cohort. He also received the Outstanding Thesis Award from the Faculty of Engineering and Applied Science for his doctoral research at UOIT.